Biogeochemistry (2023) 164:537–553
https://doi.org/10.1007/s10533-023-01056-5

Soil nitrogen availability in a temperate forest exhibits large variability at sub-tree spatial scales

Palani R. Akana · Isobel E. J. Mifsud · Duncan N. L. Menge

Received: 25 October 2022 / Accepted: 2 June 2023 / Published online: 19 June 2023
© The Author(s), under exclusive licence to Springer Nature Switzerland AG 2023

Abstract In temperate forests, the availability of soil nitrogen (N) exhibits substantial spatial variation, although the variability at small scales (10 s of cm to 10 s of m) is not well understood. We characterized the spatial patterning of soil extractable inorganic N concentrations and net N mineralization rates in two 430 m^2 plots within Black Rock Forest, New York (USA). One plot was dominated by N-fixing black locusts (*Robinia pseudoacacia*) and the second by oaks (*Quercus* spp.). The two plots exhibited similar levels of spatial inequality (10% of soil area contained 29–44% of extractable N concentrations and net N mineralization rates) and scales of spatial patterning, which was present over distances < 2.3 m. Soil total N concentrations explained spatial patterns in extractable N (adjusted $R^2 = 0.67$ and 0.34 in the oak- and locust-dominated plots) but not net N mineralization (adjusted $R^2 < 0.15$ for both plots). Extractable N concentrations in our soil cores poorly predicted extractable N in neighboring soil cores 10 cm away (adjusted $R^2 = 0.38$ and 0.63 in the oak- and locust-dominated plots), and this can generate substantial error when calculating rates of net N mineralization. Spatial inequality in soil N availability decreased substantially when soil N was aggregated across larger areas of up to several m^2, which suggests that plants with larger root systems have more equal access to soil N. Large variation in soil N availability at sub-tree spatial scales may contribute to spatial patterning in processes like belowground competition, seedling recruitment, and gaseous soil N fluxes.

Keywords Soil nitrogen cycling · Net nitrogen mineralization · Temperate forest · Spatial heterogeneity · Semivariogram · GINI coefficient

Introduction

Soil nutrients are highly variable across space (Lechowicz and Bell 1991; Jackson and Caldwell 1993b; Darrouzet-Nardi and Bowman 2011), with important implications for seedling establishment, plant growth, and overall ecosystem nutrient dynamics (Ettema and Wardle 2002; Hutchings et al. 2003). Soil nitrogen (N) availability, which hereafter refers to the concentration of extractable inorganic N and to the rate of net N mineralization, is particularly spatially variable (Lechowicz and Bell 1991; Jackson and Caldwell 1993a, b; Hutchings et al. 2003; Wang et al. 2007; Darrouzet-Nardi and Bowman 2011). For

Responsible Editor: Melanie A. Mayes.

Supplementary Information The online version contains supplementary material available at https://doi.org/10.1007/s10533-023-01056-5.

P. R. Akana (✉) · I. E. J. Mifsud · D. N. L. Menge
Department of Ecology, Evolution & Environmental Biology, Columbia University, New York, NY 10027, USA
e-mail: pra2116@columbia.edu

instance, in a sagebrush steppe ecosystem, extractable ammonium (NH_4^+) and nitrate (NO_3^-) in individual soil cores varied more than tenfold in < 1 m^2 and were concentrated in hotspots (areas of particularly high concentration) to a greater degree than plant-available phosphorus and potassium (Jackson and Caldwell 1993a, b).

The spatial scale of variability in soil nutrients is important, given that plants can only acquire soil nutrients from the area over which their roots and associated mycorrhizae extend. Most studies that have investigated the spatial patterning of soil N in forests do so at spatial scales > 5 m (Finzi et al. 1998; John et al. 2007; Wang et al. 2007; Waring et al. 2015; Liu et al. 2020), which is appropriate for individual mature trees and tree communities. For example, following the pioneering work of Zinke (1962), a growing body of research supports the idea that soil nutrients are influenced at the scale of individual canopy trees, driven by their species-specific litter chemistry (Waring et al. 2015). At slightly larger spatial scales, elevated soil N has been observed at the level of tree communities (rather than the level of individual trees), where N-rich foliage and litterfall create self-reinforcing "islands of fertility" (Osborne et al. 2020).

Despite this focus on scales > 5 m, spatial patterning of nutrient availability in forest soils also occurs at smaller scales (Lechowicz and Bell 1991; Kleb and Wilson 1997; Farley and Fitter 1999; Schimel and Bennett 2004). For instance, in a woodland site, Farley and Fitter (1999) found 2 to tenfold variation in NH_4^+ and NO_3^- concentrations at scales of only 20 cm. Such sub-tree scales of spatial patterning are relevant to a variety of community- and ecosystem-scale patterns and processes. For instance, N-rich soil microsites are related to the spatial distributions of soil faunal and microbial communities (Ettema and Wardle 2002) and hotspots of gaseous N emission from soils (Palta et al. 2014). Soil N spatial patterning can also affect plant growth and community composition. One example of this is where plant species with high foraging precision proliferate fine roots and/or mycorrhizae into nutrient-rich patches and outcompete less-responsive species (Kembel and Cahill Jr 2005; Li et al. 2017); this suggests that the degree of spatial inequality in soil N could determine which plant species are more competitive. A second example is where plants with small root systems, such as seedlings and some understory plants, sometimes fail to encounter the nutrients they require in heterogeneous soil environments (Hutchings et al. 2003). Thus, the spatial patterning of soil N could affect community composition by regulating seedling growth and acting as an abiotic filter on tree establishment (Hutchings et al. 2003; Liu et al. 2020).

A variety of factors affect soil N availability, many of which are interrelated. For example, soil C:N ratios (Pastor et al. 1984; Booth et al. 2005; Hishi et al. 2013) and soil total N concentrations (Accoe et al. 2004; Booth et al. 2005; Perakis and Sinkhorn 2011) have direct effects on soil N availability, and they in turn are affected by foliar chemistry, leading to the focus on soil N availability at the scale of mature tree canopies (Boerner and Koslowsky 1989). However, these drivers might also vary at smaller spatial scales. Foliar chemistry of understory vegetation likely operates at smaller spatial scales, as do other proximate drivers like soil water content (Hishi et al. 2013) and soil microbial hotspots (Kuzyakov and Blagodatskaya 2015) and more ultimate drivers like micro-scale variation in topography (which influences soil moisture and litter accumulation) or soil structure (Stark 1994; Todd et al. 2000; Yu et al. 2018).

To characterize spatial patterning in soil N availability on a scale relevant for seedling establishment, we measured soil concentrations of extractable N and rates of net N mineralization in two forest plots, with spatial intervals between sampled locations ranging from 0.1 to > 20 m (whereas previous research has focused mostly on scales > 5 m). To set up a contrast in ecosystem N cycling, we studied an "oak-dominated plot" where red oak (*Quercus rubra*, a non-N-fixing, ectomycorrhizal species with low foliar N) comprised > 50% tree basal area and a "locust-dominated plot" where black locust (*Robinia pseudoacacia*, a N-fixing, arbuscular mycorrhizal species with high foliar N) comprised > 50% basal area. We asked the following questions: *For soil extractable N concentrations and net N mineralization rates in our plots,* (1) *What is the scale and intensity of spatial patterning?* (2) *How does spatial patterning differ in the oak vs. locust-dominated plots?* (3) *Which environmental factors drive this spatial variability?* We hypothesized that soil N availability would be highly concentrated in hotspots and would exhibit spatial structure at scales equal to or smaller than the size of canopy trees. We expected to find higher

N availability in the locust-dominated plot, although we were unsure how elevated N would affect spatial patterning.

We found high spatial heterogeneity in both plots, even at spatial scales < 2 m, which has implications for both seedling dynamics and ecosystem ecology. Therefore, we asked two additional questions. We examined an implication for seedling establishment by asking: (4) *Based on the spatial patterning of soil N in our plots, how does a plant's effective rooting diameter affect its ability to access soil N?* Finally, we examined an implication for field measurements of net N mineralization by asking: (5) *How reliable are estimates of soil inorganic N concentrations based on neighboring soil cores 10 cm away, and can we obtain more reliable estimates from other soil variables such as total N concentration?*

Materials and methods

Site description

Our plots were located within Black Rock Forest, a 1550 ha forest preserve located in the Hudson Highlands Region of south-eastern New York (41.420° N, 74.009° W). Mean annual precipitation is around 1.2 m $year^{-1}$ and mean monthly temperatures range from approximately − 2.7 °C in January to 23.4 °C in July (Schuster et al. 2008). The forest is rocky with shallow, nutrient-poor soils, and the forest canopy is dominated by oaks (principally *Quercus rubra* and *Q. montana*) (Schuster et al. 2008).

In late summer 2020, we established two 18-by-24 m plots characterized by different plant communities (Fig. 1). The two plots were located ~ 0.3 km apart. Both plots were at ~ 300 m elevation, were on relatively flat ground (average slope < 10º), and had N deposition rates of < 1 g N m^{-2} $year^{-1}$ (National Atmospheric Deposition Program 2018). In our oak-dominated plot, *Quercus rubra* (red oak) composed 59.5% of living basal area (of stems > 1 cm diameter at 1.3 m), followed by *Quercus montana* (chestnut oak; 25.6%) and *Acer rubrum* (red maple; 7.1%). In our locust-dominated plot, *Robinia pseudoacacia* (black locust) composed 60.6% of living basal area, followed by *A. rubrum* (26.3%). The oak-dominated plot had lower total basal area of living trees: 34.0 versus 48.3 m^2 ha^{-1}; fewer intermediate-sized trees: 8 versus 27 stems with 20–40 cm diameter at breast height (1.3 m; dbh); and more large trees: 4 versus 1 stem > 40 cm dbh. The oldest trees in the locust-dominated plot were just over 60 years according to tree core data (A. Helms, unpublished data), and several recently dead locust and ash (*Fraxinus* sp.) stems were still standing. The stand age of the oak-dominated plot was thought to be between 100 and 120 years, based on the stand age of an adjacent plot from Schuster et al. (2008), and it had no large dead stems. The locust-dominated plot had greater understory cover composed primarily of barberry (which is known to affect nitrification (Kourtev et al. 1999)), blackberry, wild rose, and several grass species, all distributed patchily throughout the plot. The sparse understory in the oak-dominated plot was composed primarily of the native shrub *Kalmia latifolia*, an ericoid mycorrhizal species known to affect N cycling (Ward et al. 2021).

The soils in our plots were loamy and derived from glacial till, with those in the oak-dominated plot classified as Hollis very stony soils and those in the locust-dominated plot classified as Erie extremely stony soils (Natural Resources Conservation Service 2023). The organic horizon in the oak-dominated plot appeared slightly thicker than in the locust-dominated plot, though fine roots and organic matter were concentrated in the top few centimeters in both plots. Soils in both plots were shallow, with bedrock typically found at 10–30 cm. A large quantity of millipede frass in the leaf litter layer in the oak-dominated plot may have affected soil N cycling due to high concentrations of NH_4^+ in the millipede frass (P. Akana, unpublished data).

Soil field sampling and analysis

In each plot, 155 soil cores were collected from an 18-by-24 m grid in a sampling scheme similar to a staggered nested design (Cole 2009). Spatial intervals between cores ranged from 0.1 to > 20 m. 65 soil cores were taken in a gridded design 2.8 m apart and 90 additional cores were taken from a random x- and y-offset between 0.1–1.4 m from random non-edge samples in the grid. There was a bias toward choosing smaller offset values (0.1–0.4 m) to increase the number of cores whose pairwise distances were < 1 m. For all trees within the plot or within 2 m of the plot edge, we recorded the x- and y-coordinates (to the nearest

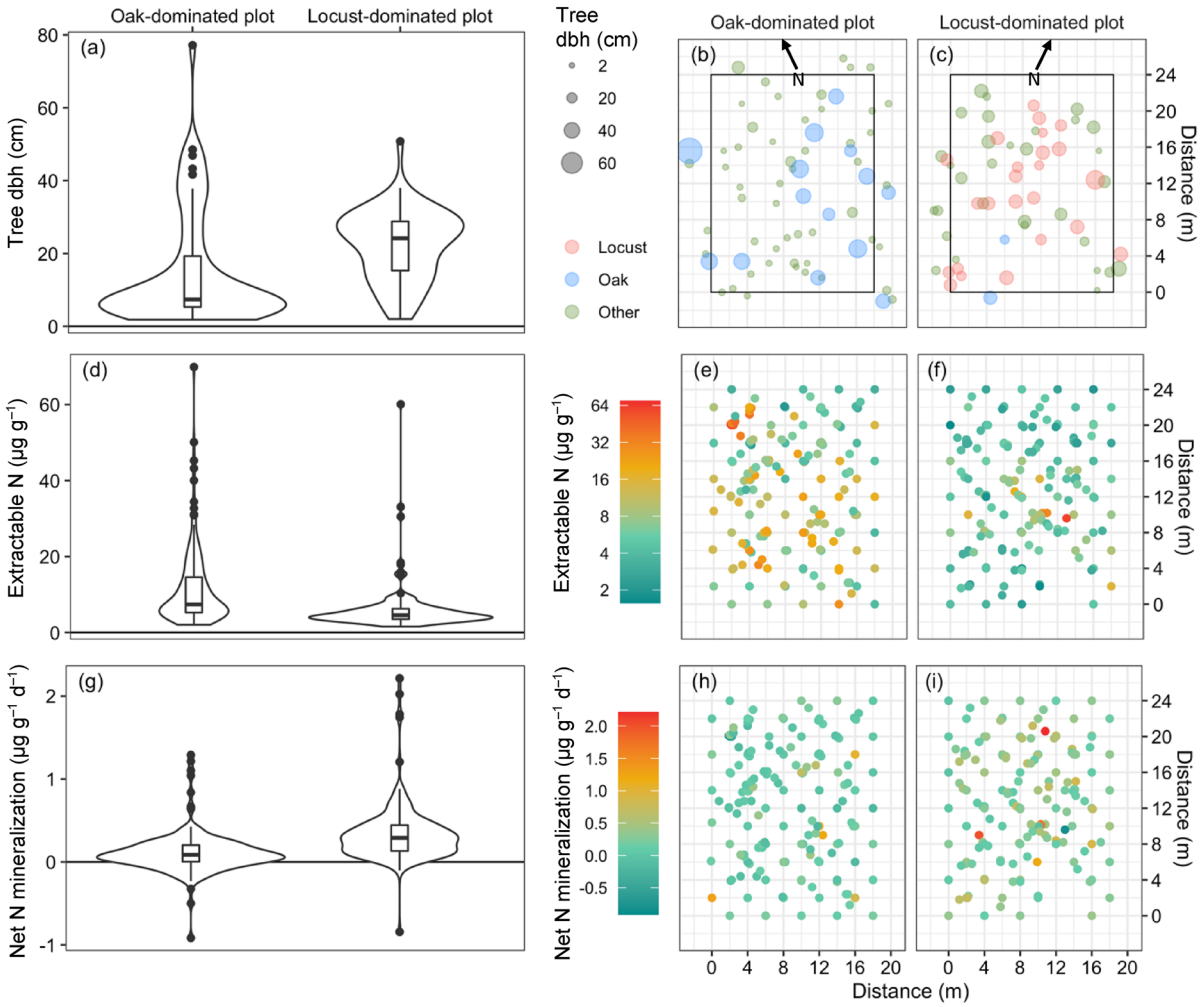

Fig. 1 Violin plots and spatial coordinates of **a**–**c** tree diameter at breast height (dbh), including trees within 2.5 m of the plot boundary, **d**–**f** soil extractable inorganic nitrogen (NH_4^+ plus NO_3^-) to 10 cm depth, and **g**–**i** net nitrogen mineralization to 10 cm depth in two forest plots characterized by different dominant tree species. Soil data are for 155 cores per plot. Violin plot widths are proportional to the number of data points; inset boxplots show median and interquartile range, with whiskers extending to the furthest datum within an additional 1.5 interquartile ranges (individual points shown beyond whiskers). Soil was sampled on a regular grid with additional randomized samples (see "Materials and methods"); the sampling gap at the bottom of the locust-dominated plot was due to a boulder patch. In (**b**, **c**) the diameter of points is proportional to tree dbh and the black rectangle delineates the plot boundary

10 cm), the dbh, and the species. The soil sampling design and the locations and sizes of trees in our plots are shown in Fig. 1.

Before collecting each soil core, we measured the depth of leaf litter (to the nearest cm), visually estimated the topographic slope (to the nearest 5°), and recorded the height (to the nearest 50 cm) and species of understory vegetation directly above the core. Soil cores were collected using a 7.3 cm diameter impact corer to a depth of 10 cm (unless large rocks restricted collection to < 10 cm). If a selected sampling location had a boulder, tree stem, or large root, the core was moved to the nearest location where soil was present. Each soil core was analyzed for extractable inorganic N (NO_3^- plus nitrite (NO_2^-), hereafter referred to as NO_3^-, and NH_4^+) and was paired with a second core 10 cm away (midpoint-to-midpoint) to determine the rate of net N mineralization. Mineralization cores

were extracted with the impact corer, wrapped in impermeable plastic clingfilm (Saran Wrap, SC Johnson, Racine WI), and placed back in the ground for 8 weeks. Extractable N (initial) cores were collected in July and early August 2020 and mineralization (final) cores were collected in late August and September 2020 (see Fig. S1 for June–October temperature and rainfall data).

We processed soil cores in the field (Keeney and Nelson 1983) by sieving to 5 mm, homogenizing, and extracting 4–6 g of soil in 30 mL of 2 M potassium chloride (KCl). Extracts were shaken for 1 h, filtered through Whatman #42 filter paper within 24 h of collection, and frozen until they were analyzed for NO_3^- and NH_4^+. Duplicate KCl extractions were performed every 15 samples. From each core, a second subsample of 4–6 g soil was oven dried at 65 °C for > 48 h to determine gravimetric water content. This second subsample was then ground and analyzed for carbon and N concentrations using an elemental analyzer (Flash 2000, Thermo Scientific, Waltham, MA, USA). NO_3^- and NH_4^+ concentrations were analyzed via colorimetry (Keeney and Nelson 1983) using a discrete analyzer (SmartChem 170, Unity Scientific, Milford, MA, USA). For simplicity, we hereafter refer to extractable NO_3^- and NH_4^+ concentrations as "extractable N". The rate of net N mineralization was calculated as final minus initial extractable N divided by time (net NO_3^- plus NH_4^+ production per mass dry soil per day), and net nitrification was calculated as final minus initial NO_3^- divided by time (net NO_3^- production per mass dry soil per day). Soil bulk density (soil dry mass, sieved to 5 mm, per total volume of the core) was calculated for the final cores.

Spatial inequality and autocorrelation

Spatial patterning encompasses both spatial inequality (i.e., the degree to which nutrients are at particularly high concentrations in some areas, hotspots, and at particularly low concentrations in other areas, 'cold' spots) and spatial autocorrelation (i.e., the degree to which one location is predictive of nearby locations). For each plot (oak- and locust-dominated) and variable of interest (extractable N and net N mineralization), we assessed the degree of spatial inequality by constructing a Lorenz curve and calculating a GINI coefficient (Gastwirth 1972). To construct a Lorenz curve, data are arranged in ascending order with respect to the variable of interest, and the cumulative percentage of data points is plotted on the x-axis against the cumulative percentage of the variable's sum on the y-axis. The GINI coefficient, a statistic of inequality, quantifies the proportion of area below the 1:1 line that lies between the Lorenz curve and the 1:1 line. GINI coefficients can range between 0 and 1, with 0 indicating perfect equality (all data points have the same value) and 1 indicating perfect inequality (only one data point is non-zero). Prior to making Lorenz curves, negative rates of net N mineralization were set to zero to reflect the new N made available through time.

We assessed the spatial autocorrelation of extractable N and net N mineralization in our plots using semivariograms, a tool that characterizes how between-sample variability changes as a function of the distance between samples (Trangmar et al. 1986; Ettema and Wardle 2002). We binned all pairs of soil cores in 0.25 m increments (the smallest distance with > 25 pairs per bin) up to a total distance of 10 m (approximately half the plot length and width). Then, within each bin, we computed the semivariance (one half the mean of the squared differences between each pair of cores) and fit exponential semivariogram models using the 'gstat' package in R. A semivariogram fits three parameters: the nugget (residual semivariance at zero distance between data points), the sill (asymptotic semivariance), and the range (the scale of spatial patterning, or the maximum distance over which spatial autocorrelation is observed). Since extractable N in both plots was highly right-skewed, we also fit semivariograms to extractable N data that had been normalized with natural-log and a Box-Cox transformations (Fig. S2). A Box-Cox transformation is common in geospatial analyses and standardizes each value according to the formula: $x_{BoxCox} = \frac{x^{\lambda}-1}{\lambda}$, where λ is selected from a set of values (we used -2 to $+2$ in 0.05 increments) so that the transformed data best conform to a normal distribution. Box-Cox transformations were done using the 'MASS' package in R.

To examine the drivers of 'within-plot' soil N availability in each plot, we ran linear regression models on extractable N and net N mineralization using a variety of predictors specific to each soil core. These predictors were gravimetric water content, total N concentration, C:N ratio, leaf litter depth, topographic slope, understory vegetation height,

tree-crowding index [for all trees within 5 m, the square of dbh divided by the square of stem distance (Canham et al. 2004; Taylor et al. 2017)], and the proportion of tree-crowding from oaks (for the oak-dominated plot) or locusts (for the locust-dominated plot). A natural-log transformation was applied to noticeably right-skewed variables, and then all variables were standardized by the z-score (the number of standard deviations from the mean) to facilitate comparison of coefficient effect sizes (coefficients of z-scored variables convey how many standard deviations the response variable will change for a one standard deviation change in a dependent variable). Additionally, we ran linear regressions on soil total N concentration in isolation (without standardizing by the z-score) because soil total N was the strongest predictor of N availability in both plots.

Plant N access

We quantified inequality in soil N availability across a gradient in spatial resolution of soil area, where the sampled area represented the soil N accessible to understory plants with a given rooting area. This approach enabled us to examine how variation in N access by understory plants may be affected by both root system area and soil N spatial patterning. For each combination of plot (oak- and locust-dominated) and N metric (extractable N and net N mineralization), we simulated 100 spatially-explicit grids of soil N availability; each grid contained 40,000 cells and had the same scale of spatial patterning as our field data (Fig. S3). For each simulated grid, we quantified inequality at three different spatial resolutions with Lorenz curves and GINI coefficients: square 6.5-by-6.5 cm grid cells (or 0.004 m^2; the area sampled by the soil corer) were aggregated into larger patches of 5 and 40 times the length and width of grid cells (or approximately 0.1 and 6.8 m^2 of soil area). See SI Text for more details.

Extractable N variability between neighboring soil cores

Typically, when making field measurements of net N mineralization, the common practice is to estimate the initial extractable N in the mineralization core by assuming it is equal to the extractable N in a neighboring soil core (Binkley and Hart 1989). The validity of this assumption relies on the presence of strong spatial autocorrelation in extractable N at the spatial scale equal to the distance between the mineralization cores and their neighboring cores (usually ~ 10 cm). In the oak-dominated plot, the variance in extractable N at 10 cm was high, so we decided to examine the accuracy of the assumption that neighboring cores contain similar amounts of extractable N. To do this, we compared the neighboring core method to a method where extractable N was estimated from a linear regression on soil total N. The accuracy of two methods in our two plots was assessed by their R^2-values (Table 4), which were calculated as $1-\frac{residual\ variance}{total\ variance}$. For the neighboring core method, the residual variance was found by determining the variance in extractable N at 10 cm from the fitted semivariogram models. For the linear regression method, extractable N and total N were transformed by their natural log for the linear regression, and then data were back-transformed to compute residual variance. We used the estimates of initial extractable N from the regression on total N to recalculate rates of net N mineralization, which were compared to the rates calculated from the neighboring core method. We also reran our spatial autocorrelation analysis on the recalculated rates.

All analyses were conducted in R version 4.0.2 (R Core Team 2020).

Results

Plot-level soil characteristics

Surface soils to 10 cm depth in the oak-dominated plot had 140% higher carbon concentrations and 59% higher N concentrations than in the locust-dominated plot (Table 1). In addition, surface soil extractable N was 96% higher in the oak-dominated plot (arithmetic mean ± SD of 11.7 ± 10.1 versus 5.98 ± 6.06 μg N g^{-1}; all reported values are per gram soil dry mass). The oak-dominated plot had threefold lower average rates of net N mineralization (0.11 ± 0.25 versus 0.34 ± 0.35 μg N g^{-1} d^{-1}), likely driven by higher soil C:N ratios (Table 1). Net immobilization of N (higher initial than final concentrations of extractable N) was observed in 24% of the oak-dominated soil cores and only 2.6% of the locust-dominated cores. The oak-dominated plot exhibited no net nitrification

Table 1 Selected soil properties (arithmetic mean ± standard deviation) and tree basal area

Variable	Oak-dominated plot	Locust-dominated plot
Extractable inorganic N (μg g^{-1})	11.7 ± 10.1	6.0 ± 6.1
Net N mineralization (μg g^{-1} day^{-1})	0.11 ± 0.25	0.34 ± 0.35
Net nitrification (μg g^{-1} day^{-1})	–0.003 ± 0.009	0.22 ± 0.22
Soil total N (% mass)	0.62 ± 0.32	0.39 ± 0.20
Soil total C (% mass)	16.5 ± 9.4	6.8 ± 3.1
Soil C:N ratio (by mass)	25.9 ± 3.1: 1	17.9 ± 3.4: 1
Soil moisture (% mass)	28.5 ± 10.7	26.3 ± 6.2
Litter depth (cm)	2.6 ± 1.6	3.2 ± 1.2
Bulk density (kg m^{-3})	349 ± 120	576 ± 133
Tree basal area (m^2 ha^{-1})	34.0	48.3

(−0.003 ± 0.009 μg N g^{-1} day^{-1}), whereas the locust-dominated plot exhibited net nitrification of 0.22 ± 0.22 μg N g^{-1} day^{-1}. Bulk density was 65% higher in the locust-dominated plot (Table 1), meaning that on a soil volume-basis, between-plot differences in total N and extractable N would be smaller than reported here, whereas differences in net N mineralization and net nitrification would be greater.

Spatial patterning of soil N

In both plots, soil N availability exhibited a high degree of inequality among soil cores. Net N mineralization exhibited greater inequality than extractable N, which in turn was more unequal than total N (Fig. 2). For net N mineralization, the oak-dominated plot had a larger GINI coefficient than the locust-dominated plot (0.63 versus 0.44). The richest 10% of soil cores (i.e., the 10% of cores with the highest net N mineralization rates) accounted for 43.7% of net N mineralization rates across all cores in the oak-dominated plot, whereas the richest 10% of cores accounted for 31.9% of net N mineralization rates in the locust-dominated plot. Greater inequality in the oak-dominated plot was caused, in part, by net N immobilization in 24% of soil cores, in which no new inorganic N was released. Extractable N exhibited slightly greater inequality in the oak-dominated plot than in the locust-dominated plot (GINI coefficients of 0.41 versus 0.35; coefficients of variation of 1.01 versus 0.86), but was similarly concentrated in hotspots, with the richest 10% of soil cores accounting for 30% of extractable N concentrations. Total N had GINI coefficients of 0.27 and 0.21 in the oak- and locust-dominated plots, and the richest 10% of soil cores accounted for 23% and 21% of soil N concentrations, respectively.

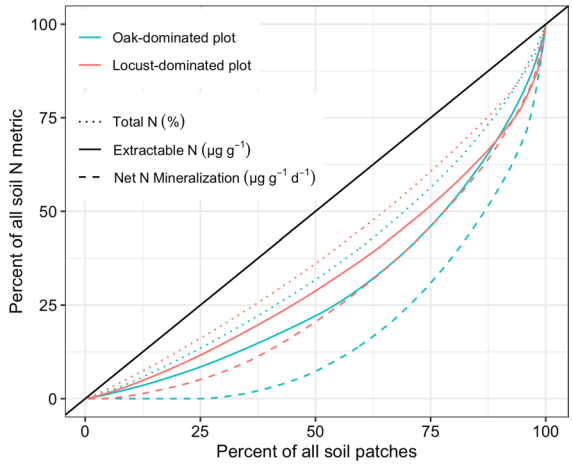

Fig. 2 Lorenz curves showing the inequality of total N (dotted curves), extractable N (solid curves) and net N mineralization (dashed curves) in soil cores from two plots characterized by different dominant tree species. Each curve connects data from 155 soil cores. Negative values of net N mineralization were set to zero (see Text). The area between the curves and the black 1:1 line denotes between-core inequality in the soil N metrics. GINI coefficients are given in Table 2

Spatial autocorrelation was detected in both plots and was stronger for extractable N than net N mineralization (Fig. 3). The spatial scale in extractable N (i.e., the maximum distance between soil cores where spatial autocorrelation was observed) was 2.3 and 1.9 m in the oak- and locust-dominated plots, respectively (Fig. 3c, d). In the oak-dominated plot, extractable N values between cores 0.1 m apart (the smallest distance between cores) were 33% as variable as between cores beyond the spatial scale of 2.3 m,

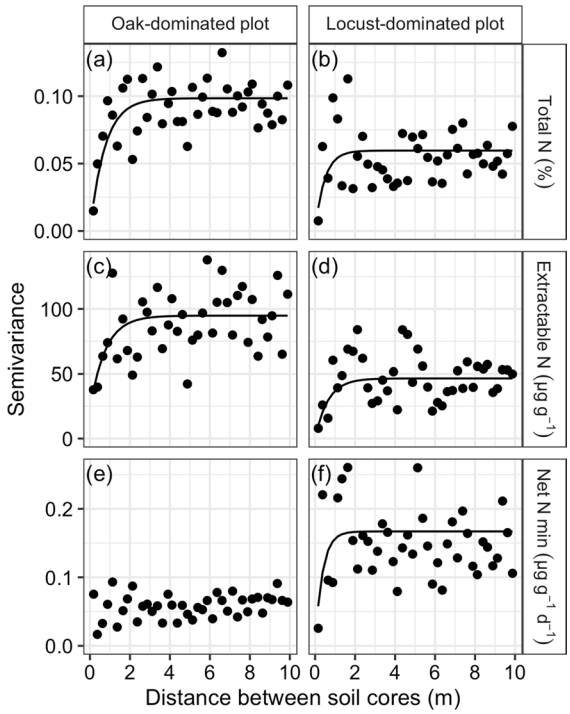

Fig. 3 Semivariograms of soil total N (**a**, **b**) extractable N (**c**, **d**) and net N mineralization (**e**, **f**) in two forest plots characterized by different dominant tree species. Data are binned in 0.25 m distance increments. Each point shows the mean semivariance of the > 25 pairwise comparisons between soil cores within the distance bin. Curves are shown if an exponential semivariogram model converged using the R package 'gstat'

whereas in the locust-dominated plot, cores 0.1 m apart were only 14% as variable as cores beyond the spatial scale (Table 2). For net N mineralization, the oak-dominated plot exhibited no spatial autocorrelation (Fig. 3e), meaning that mineralization rates in cores 0.1 m apart were as different as cores up to 10 m apart, whereas the locust-dominated plot had a spatial scale of 1.1 m and cores 0.1 m apart were 24% as variable as cores > 1.1 m apart (Fig. 3f).

Drivers of soil N availability

Extractable N tended to be higher in soil cores with greater moisture and total N concentrations, and after accounting for these two variables, extractable N was not significantly related to tree-crowding (an index of the number, size, and proximity of nearby trees), understory vegetation height or species, nor any of the other variables we measured (Table 3). The natural log of soil total N, which was the best predictor of extractable N, by itself accounted for 68% and 35% of the variation in the natural log of extractable N in the oak- and locust-dominated plots (Fig. 4a). We investigated which environmental variables were correlated with total N concentration and found that in the oak-dominated plot, total N increased with litter depth and decreased with tree-crowding, whereas in the locust-dominated plot, total N showed no trend with litter depth and increased with tree-crowding (Fig. S4–S5). Net N mineralization was poorly predicted

Table 2 Soil N spatial patterning

Spatial patterning property	Spatial patterning metric	Total N (%)		Extractable N (µg g^{-1})		Net N min (µg g^{-1} d^{-1})	
		Oak-dominated	Locust-dominated	Oak-dominated	Locust-dominated	Oak-dominated	Locust-dominated
Spatial scale	SVG range	2.2 m	1.4 m	2.3 m	1.9 m	< 0.25 m	1.1 m
% of max variability[a]	@ 0.1 m	13%	19%	33%	14%	100%	24%
	@ 0.25 m	29%	42%	45%	32%	100%	50%
	@ 1 m	74%	88%	79%	79%	100%	94%
Inequality	GINI	0.27	0.21	0.41	0.34	0.63	0.44
	25% cores[b]	44%	39%	54%	48%	69%	54%
	10% cores[b]	23%	21%	30%	30%	44%	32%
	2% cores[b]	6%	8%	10%	14%	19%	13%

SVG semivariogram

[a]Percent of max variability calculated as $100 * \frac{semivariance\ at\ the\ given\ distance}{semivariance\ at\ the\ sill}$

[b]Percentage of soil N metric contained in the specified percentage of soil cores with the greatest amount of the N metric

Table 3 R^2-values and variable coefficients for linear regression models of extractable N and net N mineralization

Metric	Plot	Adj. R^2	Variable	Standardized[a] Coefficient ± SE	Coefficient ± SE	*P*-value
Natural log of extractable N (μg g^{-1})	Oak-dominated	0.74	ln(total N) (%)	0.58 ± 0.08	0.90 ± 0.12	5.2×10^{-12}*
			Soil water (%)	0.35 ± 0.08	0.023 ± 0.005	9.1×10^{-6}*
			Veg height (cm)	− 0.092 ± 0.046	− 0.0041 ± 0.0021	0.048
			Slope (°)	− 0.092 ± 0.044	− 0.016 ± 0.007	0.037
			C:N ratio	− 0.030 ± 0.047	− 0.0070 ± 0.0109	0.520
			TCI prop. oak	0.028 ± 0.054	0.052 ± 0.101	0.610
			Litter depth (cm)	− 0.018 ± 0.051	− 0.0078 ± 0.0221	0.725
			Intercept	− 0.0064 ± 0.0409	2.3 ± 0.4	4.6×10^{-8}*
			ln(TCI)	0.0054 ± 0.0551	0.0033 ± 0.0335	0.922
	Locust-dominated	0.47	ln(total N) (%)	0.52 ± 0.09	0.79 ± 0.14	1.5×10^{-7}*
			Soil water (%)	0.26 ± 0.08	0.023 ± 0.007	0.001*
			ln(TCI)	0.11 ± 0.08	0.052 ± 0.037	0.167
			C:N ratio	− 0.068 ± 0.061	− 0.011 ± 0.01	0.264
			Slope (°)	− 0.045 ± 0.061	− 0.0066 ± 0.0089	0.462
			TCI prop. locust	− 0.018 ± 0.066	− 0.031 ± 0.115	0.789
			Veg height (cm)	0.016 ± 0.065	0.00015 ± 0.00064	0.810
			Litter depth (cm)	− 0.012 ± 0.063	− 0.0055 ± 0.0281	0.845
			Intercept	0.0044 ± 0.0575	2.2 ± 0.4	2.2×10^{-8}*
Net N min. (μg g^{-1} d^{-1})	Oak-dominated	0.002	Intercept	0.11 ± 0.02	0.28 ± 0.24	0.241
			TCI prop. oak	0.033 ± 0.025	0.087 ± 0.067	0.197
			C:N ratio	− 0.021 ± 0.022	− 0.0069 ± 0.0075	0.359
			ln(TCI)	0.020 ± 0.026	0.017 ± 0.023	0.456
			ln(total N) (%)	0.018 ± 0.054	0.036 ± 0.109	0.743
			Veg height (cm)	0.013 ± 0.022	0.00079 ± 0.00141	0.576
			Slope (°)	− 0.0056 ± 0.0227	− 0.0013 ± 0.0054	0.806
			Soil water (%)	0.0014 ± 0.0526	0.00013 ± 0.00491	0.979
			Litter depth (cm)	− 0.0004 ± 0.025	− 0.0002 ± 0.0156	0.989
	Locust-dominated	0.12	Intercept	0.33 ± 0.03	0.80 ± 0.27	0.003*
			ln(total N) (%)	0.13 ± 0.04	0.40 ± 0.12	0.001*
			Veg height (cm)	0.050 ± 0.031	0.00088 ± 0.00055	0.109
			Soil water (%)	− 0.029 ± 0.037	− 0.0045 ± 0.0057	0.437
			Litter depth (cm)	0.027 ± 0.028	0.022 ± 0.023	0.340
			TCI prop. locust	0.019 ± 0.03	0.061 ± 0.096	0.528
			C:N ratio	− 0.015 ± 0.029	− 0.0036 ± 0.0066	0.591
			ln(TCI)	0.014 ± 0.032	0.013 ± 0.029	0.661
			Slope (°)	− 0.0014 ± 0.0283	− 0.0004 ± 0.0076	0.960

TCI tree-crowding index, also known as neighborhood crowding index (NCI)

P-value significance ('*') shown for $P < 0.01$; intercept *P*-values are from linear regressions using the unscaled variables (all other *P*-values are the same when using scaled and unscaled variables)

[a]We report the coefficients ± SE for variables standardized by the z-score (number of standard deviations from the mean) and the coefficients ± SE for unscaled variables. To facilitate comparison of coefficient effect sizes, dependent variables are arranged in descending order of the absolute value of z-scored coefficients

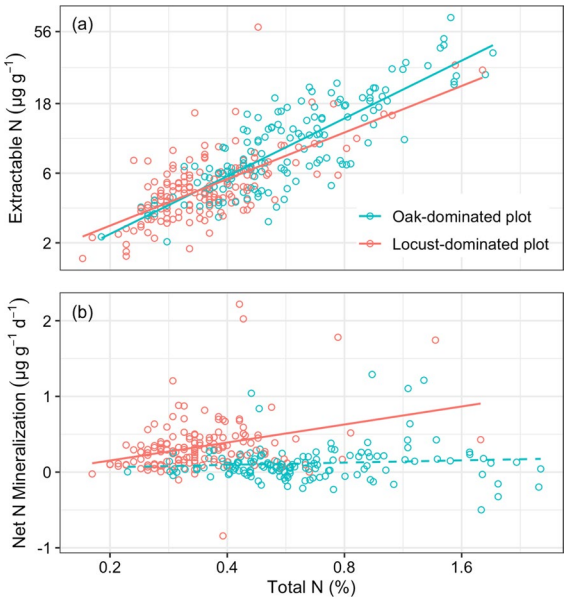

Fig. 4 Relationship between soil total N and **a** extractable N and **b** net N mineralization in two plots characterized by different dominant tree species. Significant relationships from a linear regression shown in solid lines (dashed lines for insignificant relationships). Note the log-transformed axes, except the y-axis of (**b**). The slightly different x-values are because total N is from extractable N cores in (**a**) and mineralization cores in (**b**)

by all measured covariates, which explained a mere 0.2% and 12% of the variation in the oak- and locust-dominated plots.

Inequality in N availability over varying spatial resolutions

Our simulated soil grids of extractable N and net N mineralization had similar spatial inequality as our soil core data from their respective plots (Fig. 5). Increasing the area over which soil N was aggregated decreased inequality. For instance, for extractable N simulations based on the spatial patterning in the oak-dominated plot (Fig. 5a), the richest 10% of soil patches accounted for 34 ± 3% (mean ± SD) of extractable N concentrations when soil patch area was 0.004 m^2 (the spatial resolution of our soil cores), 29 ± 3% of extractable N concentrations when patch area was increased to 0.1 m^2, and only 21 ± 4% of extractable N concentrations when patch area was further increased to 6.8 m^2 (GINI coefficients decreased from 0.40 to 0.36 to 0.19). The effect of increasing soil area leading to a decrease in the spatial inequality of soil N was greater for soil N metrics displaying less spatial autocorrelation. For example, net N mineralization in the oak-dominated plot lacked spatial autocorrelation, and the percentage of net N mineralization in the richest 10% of soil patches decreased from 33.2 ± 0.2% for 0.004 m^2 patches to 14.0 ± 0.1% for 0.1 m^2 patches to 12.5 ± 0.1% for 6.8 m^2 patches (GINI coefficients decreased from 0.59 to 0.12 to 0.01) (Fig. 5c).

Predicting extractable inorganic N

In the oak-dominated plot, extractable N was predicted substantially better by a regression on total N than by extractable N in a neighboring core 10 cm away (R^2-values of 0.68 versus 0.38), whereas in the locust-dominated plot, extractable N was predicted substantially worse by a regression on total N (R^2-values of 0.35 versus 0.63) (Table 4). When comparing these two methods for estimating initial extractable N, rates of net N mineralization differed more in the oak-dominated plot, which was the plot with less net N mineralization (Fig. 6). Interestingly, the oak-dominated plot displayed some spatial autocorrelation in net N mineralization when using the regression on total N, but not when using the neighboring core method (Fig. S6).

Discussion

Our study documented substantial spatial variability in soil N availability at the sub-tree scale (e.g., less than 5 m), a scale where the spatial patterns and drivers of soil nutrients are much less well-known than at scales of individual canopy trees or larger (Jenny 1980; Finzi et al. 1998; Lovett et al. 2004; John et al. 2007; Bateman et al. 2019). Two metrics of soil N availability, extractable inorganic N concentrations and net N mineralization rates, were concentrated in hotspots (10% of soil cores contained 29–46% of N availability) and spatially correlated up to 2.3 m at most, and even cores < 1 m apart were quite variable. Because our measurements were limited to two plots from a single time point, more data are needed to characterize patterns of spatial variation in N availability in forest soils, although the large variation in soil N availability at sub-tree spatial scales observed

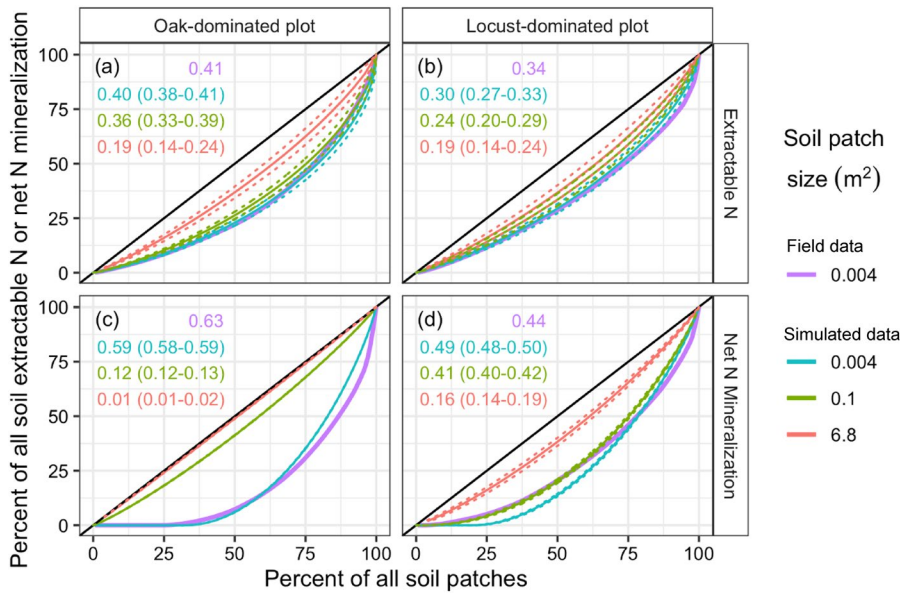

Fig. 5 Lorenz curves of field data and simulated data of **a**, **b** extractable N and **c**, **d** net N mineralization in two plots characterized by different dominant tree species. Field data, shown in purple, are described in Fig. 2. For simulated data, solid and dashed line show the mean ± SD of 100 simulations. GINI coefficients of field and simulated data (means ± SDs of Lorenz curves) are shown in the top-left of panels. Each simulation generated values for soil N availability within a 200-by-200 grid of 0.004 m^2 square soil patches (blue; 40,000 patches per simulation), which were then aggregated with neighboring patches (see Fig. S3) into square patches of 0.1 m^2 (green; 1600 patches per simulation) and 6.8 m^2 (red; 25 patches per simulation) for analysis of how soil patch size affects inequality in N availability

Table 4 Residual error and R^2-values of two methods to estimate soil extractable inorganic N (NH_4^+ plus NO_3^-)

	Neighboring cores 10 cm apart (common practice)		Linear regression on soil total N concentration	
	Residual variance	R^2	Residual variance	R^2
Oak-dominated	62.7	0.38	32.9	0.67
Locust-dominated	13.5	0.63	24.1	0.34

in our plots was consistent with previous research (Lechowicz and Bell 1991; Kleb and Wilson 1997; Farley and Fitter 1999; Schimel and Bennett 2004).

Scales and patterns of soil N spatial distributions

Our data provide novel insight into the size, prevalence, and spatial patterning of soil N hotspots in a temperate forest. Many studies on soil N spatial patterning focus on autocorrelation and ignore inequality such that there exist few published values for GINI coefficients. For extractable N, one study reported GINI coefficients of 0.59–0.73 in an alpine-subalpine ecosystem (Darrouzet-Nardi and Bowman 2011). Compared to our temperate forest plots (GINI = 0.34–0.41), we suspect that the greater inequality in extractable N in the alpine-subalpine ecosystem was likely due to patchy vegetation creating hotspots of soil N cycling.

In our plots, the scale of spatial patterning in soil N availability was 2.3 m or less, depending on the plot and N availability metric (Fig. 3c–f). This was similar to the scale of patterning in soil NO_3^- in a Canadian temperate forest (< 2 m) (Lechowicz and Bell 1991), and additional studies suggest that subtree, and even sub-meter, spatial heterogeneity in N availability may be common in temperate forests. One study found CVs of 1.0–1.2 for extractable N along 90 cm transects of 10 soil cores per transect (Kleb and Wilson 1997), similar to the CVs in extractable N for our entire 18-by-24 m plots, and another study found 2–10 fold variation in NH_4^+ and NO_3^- concentrations at scales of 20 cm

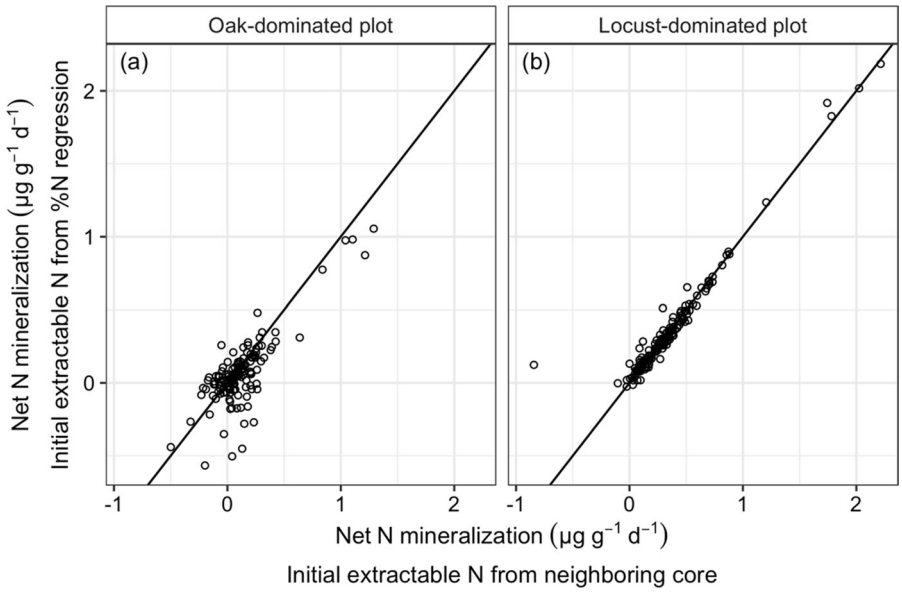

Fig. 6 Comparison of net N mineralization estimates with the initial soil N availability calculated in two ways. The traditional approach, using extractable N from a neighboring core 10 cm away, is shown on the x-axis. An alternate approach, estimating initial N from a linear regression on soil total N, is shown on the y-axis. Data shown are from 155 mineralization cores each in **a** the oak-dominated plot and **b** the locust-dominated plot. The 1:1 line is shown to facilitate comparison of methods

(Farley and Fitter 1999). For net N mineralization, the scale of spatial patterning was smaller than for extractable N, a finding supported by other studies (Jackson and Caldwell 1993a; Wang et al. 2007) and implying that N mineralization hotspots are even smaller than extractable N hotspots. In fact, in the oak-dominated plot, the scale of spatial patterning was < 0.25 m, meaning that net N mineralization was about as variable within $\frac{1}{16}$ m^2 as within the entire 430 m^2 plot (Fig. 3e). Hotspots of soil microbial activity often occur on spatial scales of μm to cm (Grundmann and Debouzie 2000; Kuzyakov and Blagodatskaya 2015), such that microsites of microbial immobilization could contribute to the lack of observable spatial structure in net N mineralization.

Wang et al. (2007) reported scales of spatial patterning of 21–55 m for NO_3^- and NH_4^+ in a temperate forest in China, although they couldn't quantify spatial autocorrelation at scales less than their 5 m sampling resolution. This could suggest that spatial patterning in extractable N exists at multiple scales; perhaps variation in microbial processes and microtopography drives extractable N at scales < 2 m, whereas variation in community structure and macro-topography drives patterns in extractable N at scales > 10 m.

Drivers of soil N spatial variability

Given that our two plots were selected to set up a contrast in soil N cycling, it was unsurprising that they differed in soil N availability. Multiple reasons could explain why the oak-dominated plot had higher average extractable N but lower average net N mineralization and net nitrification (Table 1, Fig. 1). The different tree and understory communities are clearly important, since they lead to differences in litter chemistry (lower C:N ratios in the locust-dominated plot could drive N mineralization), mycorrhizal associations (ectomycorrhizal associations in the oak-dominated plot could drive organic N cycling and suppress mineralization), and soil inorganic N uptake rates (likely higher in the locust-dominated plot, which could deplete soil extractable N). Other potentially important differences between plots include variation in soil properties, such as the thicker organic horizon and the greater abundance of NH_4^+-rich millipede frass in the oak-dominated plot. With only two plots, though, we cannot test which of these or other mechanisms drive the between-plot differences in soil N availability, so we focus hereafter on the drivers of within-plot spatial variation.

Our findings that soil moisture and total N concentration were good predictors of within-plot

variation in extractable N (Table 3) are consistent with our understanding of the proximate controls on soil N availability, since soil moisture facilitates decomposition and microbial activity (Hishi et al. 2013) and total N concentration sets the amount of N available to be mineralized (Accoe et al. 2004; Booth et al. 2005; Perakis and Sinkhorn 2011). Additionally, total N exhibited spatial autocorrelation over similar scales as extractable N (Fig. 3a–d), suggesting that the size of total N hotspots and cold spots may control the size of extractable N hotspots and cold spots. However, we note that the removal of soil inorganic N via plant and microbial uptake were likely also important drivers of within-plot variation in extractable N.

Soil total N, however, was a poor predictor of net N mineralization in both plots (Table 2), which contrasted with previous studies (Booth et al. 2005): for instance, total N accounted for 87% of the variation in net N mineralization across a soil N gradient of 9 forest sites in Oregon (Perakis and Sinkhorn 2011). The lack of correlation that we observed was not due to low variation in soil total N (the 0.2–1.9% range within our plots was larger than the 0.3–0.8% range in site means observed by Perakis and Sinkhorn (2011)) but could have been due to low net N mineralization rates (our plot means of 0.11 and 0.34 μg N g^{-1} d^{-1} were below average for temperate forests (Colman and Schimel 2013, Urakawa et al. 2016)). Low mineralization rates could be attributed to our late summer sampling missing seasonal peaks in N mineralization (Nadelhoffer et al. 1984) or to a mild preceding winter which may have reduced microbial populations by increasing freeze–thaw cycles (Durán et al. 2016). As discussed below, uncertainty in net N mineralization is increased when mineralization rates are low due to error propagation when estimating initial extractable N, and this could obscure the relationship with total N. Thus, it is likely that the true relationship between soil total N and net N mineralization in our plots is stronger than it appears. Nevertheless, because soil microbial populations exhibit short-lived fluctuations on scales of μm to cm (Kuzyakov and Blagodatskaya 2015), soil total N concentration may be only loosely associated with net N mineralization at within-plot spatial scales, especially when mineralization is only measured over a couple months, as in our study (as opposed to being integrated over an entire growing season or longer).

Although plant communities likely affected soil N availability at the plot-level (Fig. 1), within-plot effects of canopy and understory species were much more subtle. For instance, after accounting for soil moisture and total N concentration, tree-crowding and understory vegetation were not significantly correlated with either metric for N availability (Table 3). However, soil total N concentration (the strongest driver of extractable N) was facilitated by tree-crowding in the locust-dominated plot but inhibited by tree-crowding in the oak-dominated plot (Figs. S4–S5). This contrast may have been due to N-rich locust leaf litter settling close to locust stems, whereas in the oak-dominated plot, soil total N showed a stronger correlation with leaf litter depth, which tended to be lower near tree trunks. In the oak-dominated plot, high extractable N was observed in a cluster of cores with highly-organic soil which were located several meters from any oak trees (Fig. 1), though we suspect that this hotspot of extractable N was not due to a diminished influence of oak presence on soil N cycling (three large oaks outside the plot were near this area, oak leaf litter was found throughout the plot, and roots often extend many meters from tree trunks).

For total N, extractable N, and net N mineralization, the degree of spatial inequality and autocorrelation did not differ dramatically between plots, with one notable exception (Figs. 2, 3, Table 2): spatial inequality in net N mineralization was greater in the oak-dominated plot, with the richest 10% of soil cores accounting for 46% compared to 31% of net N mineralization rates. This discrepancy was likely due to lower average net N mineralization and more soil cores exhibiting net N immobilization. Similarly, other studies have found a 'dilution effect' of increased N availability on the spatial patterning of extractable soil N in a temperate forest (Yan et al. 2010) or of microbial communities in a steppe meadow (Wang et al. 2021).

Plant access to spatially-variable soil N

Spatial patterning in soil N availability can affect the growth and survival of young trees (Yan et al. 2010; Liu et al. 2020) and understory plants (Cassidy et al. 2004), with greater impact when lateral root spread is small relative to the distance between soil N hotspots (Hutchings et al. 2003). Using the scales of spatial patterning in soil N availability

(i.e., the ranges of the semivariograms) to infer soil N inequality at spatial resolutions larger than the area of our soil cores (see "Materials and methods"), we can speculate about the degree of variation in N access experienced by trees and understory plants, whose roots can span many soil cores. Our soil N simulations revealed that inequality in N access in surface soils was large at the resolution of field sampling (0.004 m^2) and declined as soil area increased (Fig. 5). This decrease occurred faster when the metric of soil N availability lacked spatial autocorrelation, as for net N mineralization in the oak-dominated plot (Fig. 5d), meaning that without spatial patterning, a plant's location will have limited impact on N access because its roots are likely to encounter both hotspots and cold spots. Thus, our results suggest that for small plants with limiting rooting distributions (e.g., newly germinated plants), N access is highly dependent on a plant's location. Even for plants with moderate rooting distributions of several m^2 (e.g., saplings and shrubs), N access can be quite variable and location-dependent when soil N availability exhibits spatial autocorrelation.

The degree to which access to soil N affects the growth of understory plants and young trees remains an open question. Although light is often more limiting than N to seedling growth (Finzi and Canham 2000), N can be important (Bigelow and Canham 2002, 2007), especially when light is plentiful or when N is particularly scarce. Yan et al. (2010) found greater numbers of *Picea* seedlings in soil with high NH_4^+ availability in a 0.25 ha forest plot with low N availability but not in a nearby plot with high N availability. Similarly, Liu et al. (2020) found only a weak relationship between *Pinus taiwanensis* seedling regeneration and extractable N concentrations in a 1 ha forest plot. However, such studies may underestimate the true effect of N on growth, since measuring N availability in a few soil cores is likely a poor approximation of the actual N accessible by a plant's roots, given the large degree of small-scale spatial variation that characterizes soil N distributions. Our soil N simulations show that plant N access can be highly variable, which suggests that soil N hotspots may be important for competition between understory plants.

Field measurements of net N mineralization

The common practice of estimating the initial extractable N in a mineralization core from a neighboring soil core relies on the presence of substantial spatial autocorrelation. In fact, the extractable N in neighboring cores must be *more than twice as similar* as between random, non-neighboring cores (i.e., the semivariance of neighboring samples is < 50% of the sill) for neighboring cores to give any predictive benefit. (Otherwise, using neighboring cores gives an $R^2 < 0$, since residual error is the sum of *squared* differences between the estimates and the data; see SI Text for additional details.) Neighboring cores must be even more similar if they are to outperform a model that estimates extractable N from correlated variables; for example, neighboring cores must be more than four times as similar (semivariance of neighboring samples < 25% of the sill) to predict extractable N with an R^2 of 0.5.

Our small-scale spatial data on extractable N concentrations provide valuable insight into the reliability of using neighboring cores to predict initial extractable N in mineralization cores. In our locust-dominated plot, extractable N was better predicted from neighboring cores than by a linear regression on total N, but the opposite was true in the oak-dominated plot (Table 4). This suggests that the reliability of neighboring cores varies by location, with less error in some plots than in others. Our findings were similar to a study in a temperate beech-maple forest, where the semivariance of the natural log of soil NO_3^- concentrations at 10 cm was between 25 and 50% of the sill (Lechowicz and Bell 1991), meaning that estimating $\ln(NO_3^-)$ from a neighboring core was better than using the mean but worse than a regression model with an $R^2 = 0.5$. As in our plots, total N can be a strong predictor of extractable N (Darrouzet-Nardi and Bowman 2011), and may be a good candidate for estimating extractable N given that it can be easily measured and should change very little while the mineralization core incubates. Furthermore, if the number of mineralization cores is large, estimating initial extractable N from total N could be achieved with fewer soil cores than the method using neighboring cores. While this discussion focuses on using soil total N concentrations to estimate initial extractable N, there are various other methods (such as

increasing incubation time or using multiple "initial" cores for each mineralization core) that could also reduce error in field estimates of net N mineralization. When net N mineralization rates are low, as in the oak-dominated plot, the method of estimating initial extractable N can have a large effect on the estimated rates (Fig. 6) and spatial patterning (Fig. S6) of net N mineralization.

Conclusion

In soil cores from our two forest plots, spatial inequality was high for both extractable N and net N mineralization, and spatial autocorrelation was only detected at spatial scales < 2.3 m. Even at these scales, autocorrelation was not particularly strong. If neighboring soil cores exhibit high variability in extractable N concentrations, as in our oak-dominated plot, estimates of net N mineralization in the field may be inaccurate due to error with estimating initial extractable N from a neighboring core. If the small-scale variation in soil N availability observed in our plots is consistent across forests, there are a variety of implications for belowground competition, soil microbial communities, gaseous N emissions, and plant N access. For instance, as we demonstrated through simulations, plant access to soil N may be strongly affected by whether or not a plant recruits in a soil N hotspot, and this could in turn drive spatial patterns of plant establishment.

Acknowledgements We thank William Schuster, Katherine Terlizzi, Matthew Munson, and other Black Rock Forest staff for field and technical assistance. Funding was provided by the David Redden Conservation Science Fund and Black Rock Forest. PRA was supported by the National Science Foundation Graduate Research Fellowship Program under Grant No. DGE 2036197.

Author contributions PA and DM designed the experiment. Data collection was performed by PA and IM. PA analyzed the data and wrote the first draft of the manuscript. All authors edited the manuscript and approved the final version.

Funding Funding was provided by Black Rock Forest through the David Redden Conservation Science Fund Small Grants Program. Palani Akana was supported by the National Science Foundation Graduate Research Fellowship Program under Grant No. DGE 2036197. Any opinions, findings, and conclusions or recommendations expressed in this material are those of the authors and do not necessarily reflect the views of the National Science Foundation.

Data availability The data collected and analyzed in this study are publicly available online at https://github.com/palakana93/Black-Rock-Forest-soil-nitrogen.

Declarations

Conflict of Interest The authors have no relevant financial or non-financial interests to disclose.

References

Accoe F, Boeckx P, Busschaert J, Hofman G, Van Cleemput O (2004) Gross N transformation rates and net N mineralisation rates related to the C and N contents of soil organic matter fractions in grassland soils of different age. Soil Biol Biochem 36:2075–2087

Bateman JB, Chadwick OA, Vitousek PM (2019) Quantitative analysis of pedogenic thresholds and domains in volcanic soils. Ecosystems 22:1633–1649

Bigelow SW, Canham CD (2002) Community organization of tree species along soil gradients in a north-eastern USA forest. J Ecol 90:188–200

Bigelow SW, Canham CD (2007) Nutrient limitation of juvenile trees in a northern hardwood forest: calcium and nitrate are preeminent. For Ecol Manag 243:310–319

Binkley D, Hart SC (1989) The components of nitrogen availability assessments in forest soils. Adv Soil Sci 10:57–112

Boerner REJ, Koslowsky SD (1989) Microsite variations in soil chemistry and nitrogen mineralization in a beech-maple forest. Soil Biol Biochem 21:795–801

Booth MS, Stark JM, Rastetter E (2005) Controls on nitrogen cycling in terrestrial ecosystems: a synthetic analysis of literature data. Ecol Monogr 75:139–157

Canham CD, LePage PT, Coates KD (2004) A neighborhood analysis of canopy tree competition: effects of shading versus crowding. Can J for Res 34:778–787

Cassidy TM, Fownes JH, Harrington RA (2004) Nitrogen limits an invasive perennial shrub in forest understory. Biol Invasions 6:113–121

Cole RG (2009) Staggered nested designs to assess scales of variability: the advantages of a spatially explicit analysis. Environ Monit Assess 153:427–434

Colman BP, Schimel JP (2013) Drivers of microbial respiration and net N mineralization at the continental scale. Soil Biol Biochem 60:65–76

Darrouzet-Nardi A, Bowman WD (2011) Hot spots of inorganic nitrogen availability in an alpine-subalpine ecosystem, colorado front range. Ecosystems 14:848–863

Durán J, Morse JL, Groffman PM, Campbell JL, Christenson LM, Driscoll CT, Fahey TJ, Fisk MC, Likens GE, Melillo JM (2016) Climate change decreases nitrogen pools and mineralization rates in northern hardwood forests. Ecosphere 7(3):1–13

Ettema CH, Wardle DA (2002) Spatial soil ecology. Trends Ecol Evol 17:177–183

Farley RA, Fitter AH (1999) Temporal and spatial variation in soil resources in a deciduous woodland. J Ecol 87:688–696

Finzi AC, Canham CD (2000) Sapling growth in response to light and nitrogen availability in a southern New England forest. For Ecol Manag 131:153–165

Finzi AC, Van Breemen N, Canham CD (1998) Canopy tree–soil interactions within temperate forests: species effects on soil carbon and nitrogen. Ecol Appl 8:440–446

Gastwirth JL (1972) The estimation of the Lorenz curve and Gini index. Rev Econ Stat 54:306–316

Grundmann GL, Debouzie D (2000) Geostatistical analysis of the distribution of NH4+ and NO2−-oxidizing bacteria and serotypes at the millimeter scale along a soil transect. FEMS Microbiol Ecol 34:57–62

Hishi T, Urakawa R, Tashiro N, Maeda Y, Shibata H (2013) Seasonality of factors controlling N mineralization rates among slope positions and aspects in cool-temperate deciduous natural forests and larch plantations. Biol Fertil Soils 50:343–356

Hutchings MJ, John EA, Wijesinghe DK (2003) Toward understanding the consequences of soil heterogeneity for plant populations and communities. Ecology 84:2322–2334

Jackson RB, Caldwell MM (1993a) Geostatistical patterns of soil heterogeneity around individual perennial plants. J Ecol 81:683–692

Jackson RB, Caldwell MM (1993b) The Scale of Nutrient Heterogeneity Around Individual Plants and Its Quantification with Geostatistics. Ecology 74:612–614

Jenny H (1980) The soil resource: origin and behavior. Springer-Verlag, New York

John R, Dalling JW, Harms KE, Yavitt JB, Stallard RF, Mirabello M, Hubbell SP, Valencia R, Navarrete H, Vallejo M, Foster RB (2007) Soil nutrients influence spatial distributions of tropical tree species. Proc Natl Acad Sci 104:864

Keeney DR, Nelson DW (1983) Nitrogen-inorganic forms. In: Page AL, Miller RH, Keeney DR (eds) Methods of soil analysis: part 2 chemical and microbiological properties, 2nd edn. vol 9, pp 643–698

Kembel SW, Cahill JF Jr (2005) Plant phenotypic plasticity belowground: a phylogenetic perspective on root foraging trade-offs. Am Nat 166:216–230

Kleb HR, Wilson SD (1997) Vegetation effects on soil resource heterogeneity in prairie and forest. Am Nat 150:283–298

Kourtev PS, Huang WZ, Ehrenfeld JG (1999) Differences in earthworm densities and nitrogen dynamics in soils under exotic and native plant species. Biol Invasions 1:237–245

Kuzyakov Y, Blagodatskaya E (2015) Microbial hotspots and hot moments in soil: concept & review. Soil Biol Biochem 83:184–199

Lechowicz MJ, Bell G (1991) The ecology and genetics of fitness in forest plants. II. Microspatial heterogeneity of the edaphic environment. J Ecol 79:687–696

Li H, Liu B, McCormack ML, Ma Z, Guo D (2017) Diverse belowground resource strategies underlie plant species coexistence and spatial distribution in three grasslands along a precipitation gradient. New Phytol 216:1140–1150

Liu J, Su S, He Z, Jiang L, Gu X, Xu D, Ma R, Hong W (2020) Relationship between *Pinus taiwanensis* seedling regeneration and the spatial heterogeneity of soil nitrogen in Daiyun Mountain, southeast China. Ecol Ind 115:106398

Lovett GM, Weathers KC, Arthur MA, Schultz JC (2004) Nitrogen cycling in a northern hardwood forest: do species matter? Biogeochemistry 67:289–308

Nadelhoffer KJ, Aber JD, Melillo JM (1984) Seasonal patterns of ammonium and nitrate uptake in nine temperate forest ecosystems. Plant Soil 80:321–335

National Atmospheric Deposition Program (2018) Total deposition maps, v2018.01.

Natural Resources Conservation Service. Web Soil Survey. United States Department of Agriculture. Available online at http://websoilsurvey.sc.egov.usda.gov/. Accessed 14 Apr 2023.

Osborne BB, Nasto MK, Soper FM, Asner GP, Balzotti CS, Cleveland CC, Taylor PG, Townsend AR, Porder S (2020) Leaf litter inputs reinforce islands of nitrogen fertility in a lowland tropical forest. Biogeochemistry 147:293–306

Palta MM, Ehrenfeld JG, Groffman PM (2014) "Hotspots" and "hot moments" of denitrification in urban brownfield wetlands. Ecosystems 17:1121–1137

Pastor J, Aber JD, McClaugherty CA, Melillo JM (1984) Aboveground production and N and P cycling along a nitrogen mineralization gradient on Blackhawk Island, Wisconsin. Ecology 65:256–268

Perakis SS, Sinkhorn ER (2011) Biogeochemistry of a temperate forest nitrogen gradient. Ecology 92:1481–1491

R Core Team (2020) R: A language and environment for statistical computing. R Foundation for Statistical Computing, Vienna

Schimel JP, Bennett J (2004) Nitrogen mineralization: challenges of a changing paradigm. Ecology 85:591–602

Schuster WSF, Griffin KL, Roth H, Turnbull MH, Whitehead D, Tissue DT (2008) Changes in composition, structure and aboveground biomass over seventy-six years (1930–2006) in the Black Rock Forest, Hudson Highlands, southeastern New York State. Tree Physiol 28:537–549

Stark JM (1994) Causes of soil nutrient heterogeneity at different scales. In: Caldwell MM, Pearcy RW (eds) Exploitation of environmental heterogeneity by plants. Academic Press, Boston, pp 255–284

Taylor BN, Chazdon RL, Bachelot B, Menge DNL (2017) Nitrogen-fixing trees inhibit growth of regenerating Costa Rican rainforests. PNAS 114:8817–8822

Todd MCL, Grierson PF, Adams MA (2000) Litter cover as an index of nitrogen availability in rehabilitated mine sites. Soil Research 38:423–434

Trangmar BB, Yost RS, Uehara G (1986) Application of geostatistics to spatial studies of soil properties. Adv Agron 38:45–94

Urakawa R, Ohte N, Shibata H, Isobe K, Tateno R, Oda T, Hishi T, Fukushima K, Inagaki Y, Hirai K, Oyanagi N, Nakata M, Toda H, Kenta T, Kuroiwa M, Watanabe T, Fukuzawa K, Tokuchi N, Ugawa S, Enoki T, Nakanishi A, Saigusa N, Yamao Y, Kotani A (2016) Factors contributing to soil nitrogen mineralization and nitrification rates of forest soils in the Japanese archipelago. For Ecol Manag 361:382–396

Wang L, Mou PP, Huang J, Wang J (2007) Spatial heterogeneity of soil nitrogen in a subtropical forest in China. Plant Soil 295:137–150

Wang C, Zhang R, Vilonen L, Qu Y, Fu X, Shi B, Cui H, Gao W, Cai H, Sun W (2021) Grazing and nitrogen addition restructure the spatial heterogeneity of soil microbial community structure and enzymatic activities. Funct Ecol 35:2763–2777

Ward EB, Duguid MC, Kuebbing SE, Lendemer JC, Warren RJ, Bradford MA (2021) Ericoid mycorrhizal shrubs alter the relationship between tree mycorrhizal dominance and soil carbon and nitrogen. J Ecol 109:3524–3540

Waring BG, Álvarez-Cansino L, Barry KE, Becklund KK, Dale S, Gei MG, Keller AB, Lopez OR, Markesteijn L, Mangan S (2015) Pervasive and strong effects of plants on soil chemistry: a meta-analysis of individual plant 'Zinke' effects. Proc R Soc B Biol Sci 282:20151001

Yan H-B, Han Y-Z, Yang X-Q, Li L (2010) Spatial relevance between natural regeneration of Picea and heterogeneity of soil available nitrogen in Guandi Mountain. Chin J Appl Ecol 21:533–540

Yu B, Liu G, Liu Q, Feng J, Wang X, Han G, Huang C (2018) Effects of micro-topography and vegetation type on soil moisture in a large gully on the Loess Plateau of China. Hydrol Res 49:1255–1270

Zinke PJ (1962) The pattern of influence of individual forest trees on soil properties. Ecology 43:130–133

Publisher's Note Springer Nature remains neutral with regard to jurisdictional claims in published maps and institutional affiliations.

Springer Nature or its licensor (e.g. a society or other partner) holds exclusive rights to this article under a publishing agreement with the author(s) or other rightsholder(s); author self-archiving of the accepted manuscript version of this article is solely governed by the terms of such publishing agreement and applicable law.